(Received 17 December 2024, Accepted 11 February 2025, Scheduled 25 February 2025)

Anomalous Reflection from Hyperbolic Media

Ilya Deriy[1], Kseniia Lezhennikova[2, 3], Stanislav Glybovksi[4], Ivan Iorsh[5], Oleh Yermakov[6], Mingzhao Song[1], Redha Abdeddaim[2], Stefan Enoch[2], Pavel Belov[7], and Andrey Bogdanov[1, *]

[1] *Qingdao Innovation and Development Center, Harbin Engineering University Sansha Rd. 1777, Qingdao 266000, Shandong, China*
[2] *Aix Marseille University, CNRS, Centrale Marseille, Institut Fresnel Institut Marseille Imaging, AMUTech, Marseille 13013, France*
[3] *Multiwave Technologies AG, 3 Chemin du Pré Fleuri 1228, Geneva, Switzerland*
[4] *Independent Researcher*
[5] *Department of Physics, Engineering Physics and Astronomy Queen's University, Kingston, Ontario K7L 3N6, Canada*
[6] *Leibniz Institute of Photonic Technology, Jena, Germany*
[7] *School of Engineering, New Uzbekistan University, Movarounnahr Str. 1, 100000, Tashkent, Uzbekistan*

ABSTRACT: Despite the apparent simplicity, the problem of refraction of electromagnetic waves at the planar interface between two media has a vibrant spectrum of unusual phenomena. An example is the paradox when an electromagnetic wave impinges on the interface between a hyperbolic medium and an isotropic dielectric. At specific orientations of the optical axis of the hyperbolic medium relative to the interface, the reflected and transmitted waves can disappear entirely, which contradicts reciprocity. In this paper, we analyze the above-mentioned paradox and present its resolution by introducing infinitesimal losses in the hyperbolic medium. We show that the reflected wave exists in the form of a ghost wave, which becomes infinitely localized at the interface of the hyperbolic medium when the losses vanish. Consequently, all the reflected waves are perfectly absorbed near the interface. We support our reasoning with analytical calculations, numerical simulations, and an experiment with self-complementary metasurfaces in the microwave range.

1. INTRODUCTION

The refraction and reflection of electromagnetic waves at the planar interface between two media have been extensively studied for various systems, including nonlinear [1], anisotropic [2], chiral [3], non-local media [4], plasmonic and all-dielectric metasurfaces [5–8]. The in-plane momentum conservation governs the refraction of a plane electromagnetic wave at the interface, also known as the phase-matching condition [9]. Knowing the dispersion of all propagating and evanescent waves at a certain frequency in both media, one can find the amplitudes and directions of the refracted, reflected, and transmitted waves. The directions of the refracted (reflected, and transmitted) waves can be easily found graphically using a technique of isofrequency contours (IFCs) — the graphical solution of the dispersion equation at the certain frequency in the wave vector space (k-space) [10, 11]. The IFCs show all possible states of light in the medium at a certain frequency accessible for scattering. The curvature and topology of IFCs crucially affect the structure of transmitted and reflected waves [12, 13]. The birefringence, negative refraction, and canalization can be easily understood in terms of IFCs [14, 15].

In media with closed IFCs, electromagnetic waves can propagate in all directions, while in media with open IFCs, some propagation directions are forbidden, resulting in unusual behavior of the reflected or transmitted waves [16]. An illustrative example of a medium with an open isofrequency contour is a *hyperbolic medium* [17]. A hyperbolic medium is a highly-anisotropic material that exhibits different signs of the real part of permittivity, permeability, or imaginary part of conductivity tensor components at the same frequency [17–19]. Thus, the IFC of the hyperbolic media has the form of hyperboloids or hyperbolas in 3D and 2D cases, respectively [17]. The hyperbolic shape of the IFCs leads to the singular photonic density of states [20, 21] which determines exotic properties of the hyperbolic medium, such as negative refraction [22–24], diffractionless [25–27] and high-directional [28–30] propagation, hybrid TE-TM polarization [31, 32], magnetic polaritons [33], and many more [17]. These phenomena are widely used for several applications, including subdiffraction imaging [34, 35], in-plane hyperlensing [36], enhanced spontaneous emission [37, 38], sensing [39–41], wavefront shaping and bending [25, 31, 36], polarization and optical spin transformation [42, 43], anomalous photonic spin Hall effect [44–46], twisted optics [47–49], and mimicking of plasma media [50]. Hyperbolic media can be implemented as layered metal-dielectric structures, nanorod arrays [17, 51, 52], natural and microstructured two-dimensional materials [53–57], graphene-patterned structures [25, 36], plasmonic gratings [24], and metasurfaces [31, 58] in the visible and near-infrared spectra.

The open topology of the IFC in hyperbolic media enables a regime in which the existence of a reflected wave can be completely suppressed by properly aligning the optical axis of the hyperbolic medium relative to the interface with an isotropic di-

* Corresponding author: Andrey A. Bogdanov (a.bogdanov@hrbeu.edu.cn).

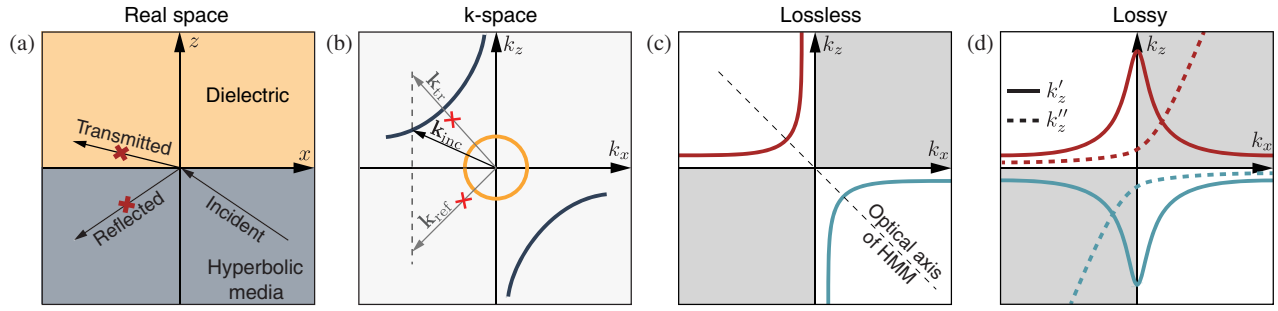

FIGURE 1. Schematic representation of the paradox that is the absence of reflected and transmitted waves in the case of refraction on the boundary between hyperbolic and isotropic media. (a), (b) Schematic representation of the refraction of a plane electromagnetic wave at the boundary between hyperbolic and isotropic media in the real space (a) and in the k-space (b). When the hyperbolic medium is lossless, and when the modulus of the k-vector in the hyperbolic medium is larger than the modulus of the k-vector in the isotropic one, by rotation of the optical axis of the hyperbolic medium, it is possible to create such a situation when there is no reflected and transmitted wave. Schematic representation of the isofrequency contour for lossless (c) and lossy (d) hyperbolic medium.

electric. This phenomenon, where the reflected field is absent, was numerically demonstrated in Refs. [59] and [60] and even inadvertently observed in Ref. [61]. However, its underlying physics remained unexplained until now.

In this work, we have, for the first time, studied in detail the *no-reflection paradox* in hyperbolic media, developed an analytical theory of anomalous reflection from hyperbolic metamaterial (HMM), and resolved the paradox through both theoretical and experimental approaches. Supported by microwave experiments, we provide a comprehensive analysis of the conditions under which this phenomenon occurs and discover its connection with *ghost waves* manifesting themselves only in a lossy medium. Our findings reveal the fundamental physics behind the absence of reflection and predict a broad angular range of perfect absorption at the interface of hyperbolic media. This discovery introduces a new physical phenomenon, offering novel opportunities for designing metamaterial-based absorbers, concentrators, and optical cavities.

2. RESULTS

2.1. No-Reflection Paradox

Let us consider the Fresnel problem for the boundary between lossless hyperbolic medium and isotropic dielectric [Fig. 1(a)]. The permittivity tensor of the hyperbolic media in the principal axes is equal to $\hat{\varepsilon} = \mathrm{diag}\,[\varepsilon_o, \varepsilon_o, -\varepsilon_e]$. The hyperbolic medium's optical axis is aligned so that asymptotic lines of the dispersion are parallel to k_x and k_z. All further results are applicable to the case of arbitrary ε_o and ε_e, but for the sake of simplicity, we put $\varepsilon_o = \varepsilon_e = \varepsilon$. Also, we draw the reader's attention to the fact that for brevity and clarity, where required, we will use the dimensionless components of the wave vector, which we mark with a tilde and define as $\tilde{k}_{x,z} = k_{x,z}/k_0$. And the real and imaginary parts of the quantities will be labeled with single and double prime respectively (e.g., $\mathrm{Re}\,[k_z] \equiv k'_z$, $\mathrm{Im}\,[k_z] \equiv k''_z$). The relation between the wavevector components in such a hyperbolic media is equal to (see Appendix A.1)

$$k_z = -\frac{1}{2}\frac{\varepsilon}{k_x}k_0^2. \tag{1}$$

Schematically, such an isofrequency contour is presented in Fig. 1(c). In the k-space, there are branches of the isofrequency contour only in two quadrants. Using the conservation of in-plane momentum, it is possible to show that (for $k_x > 0$), there is no IFC branch for the reflected wave [see Fig. 1(b)]. In addition, if the wavevector in hyperbolic media is larger than one in an isotropic dielectric, there will also be no propagating transmitted wave. As a consequence, both the reflected and transmitted waves will be absent in such a system [see Figs. 1(a) and 1(b)]. Thus, there will be a constant energy inflow due to the presence of the incident wave and no channels for its consumption (neither for dissipation nor scattering). We call the aforementioned situation as *no-reflection paradox*.

2.2. Effect of Losses

The resolution of the paradox lies in introducing losses into the system. To simplify the analytical expressions, we consider the simplest case of a lossy hyperbolic metamaterial (HMM) with isotropic losses, assuming that the imaginary parts κ of the ordinary and extraordinary components of the permittivity tensor are identical [see Eq. (A8) in the Appendix]. While derivations for a general HMM can be carried out straightforwardly, the underlying physics of the paradox becomes evident even in this simplified scenario. Under these assumptions, the permittivity tensor of the hyperbolic medium is expressed as

$$\hat{\varepsilon} = \begin{bmatrix} i\kappa & 0 & \varepsilon \\ 0 & i\kappa + \varepsilon & 0 \\ \varepsilon & 0 & i\kappa \end{bmatrix}, \tag{2}$$

where $\varepsilon, \kappa \in \mathbb{R}$.

It is important to stress that we have chosen $e^{-i\omega t}$ time dependence. Thus, $\kappa > 0$ corresponds to lossy media, while $\kappa < 0$ corresponds to media with a gain. For such a permittivity tensor, the relation between wavevector components follow

$$k_{z_\pm} = \frac{i}{\kappa}\left[k_x\varepsilon \pm \sqrt{\left(k_x^2 - i\kappa k_0^2\right)\left(\kappa^2 + \varepsilon^2\right)}\right]. \tag{3}$$

See details of the derivation in Appendix A.1.

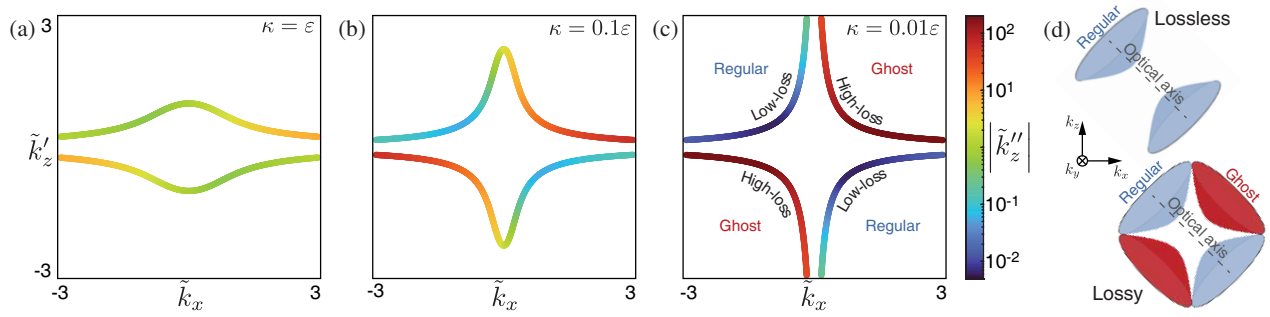

FIGURE 2. Isofrequency contours for lossy hyperbolic media with $\varepsilon = 1$ for different values of loss parameter κ: (a) $\kappa = \varepsilon$, (b) $\kappa = 0.1\varepsilon$, (c) $\kappa = 0.01\varepsilon$. Colorbar encodes the modulus of the imaginary part of $\tilde{k}_z$. Panels (a), (b), and (c) show that as $\kappa \to 0$, precisely in those quadrants in which the branches of the dispersion equation are absent for the lossless hyperbolic media, the imaginary part of k_z is going to infinity ($\mathrm{Im}\,[k_z] \to \pm\infty$). Panel (d) shows a schematic representation of the IFS for regular and ghost modes in lossless and lossy hyperbolic medium.

A schematic solution of Eq. (3) is shown in Fig. 1(d). One can see that accounting for losses results in a drastic change in the topology of the IFCs. In contrast to the lossless case, where the HMM has forbidden directions for propagating waves, the HMM with loss has no forbidden directions. The hyperbolic IFCs turn into two continuous curves spanning all four quadrants. Despite the IFCs are symmetric with respect to k_z, i.e., $k'_z(-k_x) = k'_z(k_x)$, the losses demonstrate strong asymmetry, i.e., $k''_z(-k_x) \neq k''_z(k_x)$ [see Fig. 1(d)]. Fig. 2 shows the real part of $k_{z\pm}$ from Eq. (3) as a function of k_x for a hyperbolic medium with $\varepsilon = 1$ for different values of κ. One can clearly see that in the lossy case, even for infinitesimal losses, the branches of the dispersion curves exist in each quadrant of the k-space, i.e., the waves can propagate in all directions in contrast, the well-studied lossless case of HMM [17].

The behavior of ghost waves becomes clearer by applying the power series expansion to Eq. (3) assuming $\kappa \to 0$:

$$k_{z\pm} = \pm\frac{1}{2}\left|\frac{\varepsilon}{k_x}\right| k_0^2 + \frac{i}{\kappa}\left(k_x\varepsilon \pm |k_x\varepsilon|\right) \pm i\frac{|k_x\varepsilon|}{2}\left(\frac{k_0^4}{4k_x^2} + \frac{1}{\varepsilon^2}\right)\kappa + O(\kappa^2). \quad (4)$$

The latter relation can be decomposed into two parts corresponding to the regular and ghost waves:

$$\text{Regular:}\quad k_z^{\mathrm{r}} = \underbrace{-\frac{1}{2}\frac{\varepsilon}{k_x}k_0^2}_{\text{lossless dispersion}} \underbrace{-i\kappa\frac{k_x\varepsilon}{2}\left(\frac{k_0^4}{4k_x^4} + \frac{1}{\varepsilon^2}\right)}_{\text{regular losses}}, \quad (5)$$

$$\text{Ghost:}\quad k_z^{\mathrm{g}} = \underbrace{\frac{1}{2}\frac{\varepsilon}{k_x}k_0^2}_{\text{lossless dispersion}} + \underbrace{i\frac{2k_x\varepsilon}{\kappa}}_{\text{singular losses}}, \quad (6)$$

where indices "r" and "g" correspond to the "regular" and "ghost" waves in HMM.

The key to the resolution of the no-reflection paradox lies in Eqs. (5) and (6), which clearly show the presence of dispersion branches in all quadrants of the phase space [see Figs. 2(c) and 2(d)]. One can see from Eq. (5) that for the small losses, the real part of the dispersion for the regular waves is identical to the dispersion of waves in lossless HMM, and the imaginary part is linearly proportional to the loss κ. In the limit $\kappa \to 0$, this wave becomes a regular TM mode of lossless HMM. In the general case, the dispersion of ghost waves [Eq. (6)] occupies those sectors of the k-space that are forbidden for propagation in the lossless case. In this sense, regular and ghost waves are complementary. The distinct feature between the regular and ghost waves is their losses. As one can see from Eq. (6), the imaginary part of the k_z^{g} is inversely proportional to the loss amplitude κ. This counter-intuitive relationship implies that the smaller the material losses in HMM, the larger the imaginary part of the propagation constant of the ghost waves and, therefore, the stronger their spatial localization near the HMM interface.

Figure 3 shows the refraction of a plane electromagnetic wave from the interface between lossy hyperbolic medium with $\varepsilon = 1$ and isotropic dielectric with $\varepsilon_d = 2$ for two different values of $\tilde{k}_x$. The values of $\tilde{k}_x$ are chosen so that the wavevector of the reflected waves corresponds to the ghost modes. Figs. 3(a) and 3(d) show the square modulus of the reflected field. As follows from Eq. (6), since energy is scattered (reflected) into ghost modes, the reflected field is highly decaying, and all the energy is perfectly absorbed near the HMM interface. The localization is most apparent from Fig. 3(f), where the square modulus of the reflected field is shown in logarithmic scale for different values of κ. Additional reasoning can be presented to prove the highly decaying nature of the reflected field. When the amplitudes of the incident and reflected waves are comparable, one can see the appearance of nodes and antinodes as a result of their interference. Figs. 3(b) and 3(e), where the real part of the total field is plotted, showing the absence of the interference pattern in the hyperbolic medium region, from which one can conclude that the amplitude of the reflected wave is almost negligible in comparison to the amplitude of the incident wave.

Finally, our analysis resolves the no-reflection paradox. Treating HMMs as lossless materials is inherently flawed, as it violates reciprocity for specific orientations of the optical axis relative to the HMM interface. In the lossless scenario, the ghost modes associated with reflected waves vanish from the dispersion equation because the imaginary parts of their

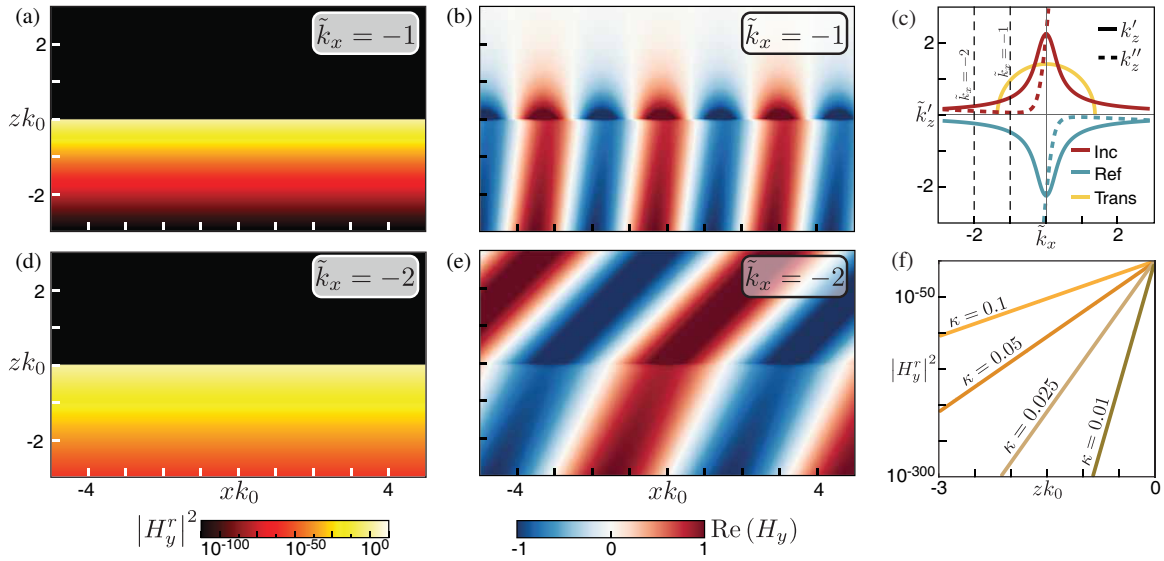

FIGURE 3. Refraction of a plane electromagnetic wave from the interface between lossy hyperbolic media with $\varepsilon = 1$ and isotropic dielectric with $\varepsilon_d = 2$ for two different values of $\tilde{k}_x = k_x/k_0$ and several values of κ. (a), (d) Modulus squared of the reflected magnetic field. (b), (e) Real part of the total magnetic field. Panels (a) and (b) correspond to $\tilde{k}_x = -2$, panels (d) and (e) correspond to $\tilde{k}_x = -1$. Panel (c) shows the k-space. All panels except (f) are plotted for $\kappa = 0.1$. Panel (f) shows the modulus squared of the reflected magnetic field for $\tilde{k}_x = -2$ and different values of κ.

propagation constants become singular. Thus, ghost modes are the critical missing element that resolves the no-reflection paradox.

2.3. Experimental Verification

For the numerical simulations and experiment, we used a self-complementary hyperbolic metasurface (a 2D analog of a hyperbolic medium with a period of 7 mm) with unit cells designed exactly as in the work [27]. While any hyperbolic medium with cut edge is suitable for the experimental verification, the self-complementary metasurface exhibits the spoof hyperbolic plasmon-polaritons at any frequency [27] being a perfect platform for the demonstration of the phenomenon under study. An FR-4 substrate with the relative permittivity $\varepsilon = 4.3$, loss tangent $\tan\delta = 0.025$, and thickness $h = 1$ mm was used to obtain the hyperbolic regime at 4 GHz [see Figs. 4(i) and 4(n)]. The two samples have been designed, having dimensions of 280 mm $\times$ 280 mm and containing 40×40 unit cells, i.e., the square sample [Fig. 4(b)] and the rhombic one [Fig. 4(c)] (with unit cells rotated by 45° relative to ones of the square sample). The excitation loop [Fig. 4(d)] of the diameter $d = 7$ mm, acting as the vertical magnetic dipole, was placed in the middle of the sample at a distance of 4 mm from the surface of the sample. A similar loop was used to measure the spatial distribution of the normal component of the magnetic field H_y. After measuring the spatial distribution, we applied the two-dimensional Fourier transform to extract the IFCs as it was done in [27, 32]. The same transform was done for the numerically calculated field maps obtained using CST Microwave Studio. For more details on the numerical simulation and experiment, see Appendix B. The numerical simulation results and the experiment for both square and rhombic structures are presented in Fig. 4. To prove the decaying nature of the reflected wave, one can resort to the same reasoning as in Section 2.2. Figs. 4(e) and 4(g) show the absolute value of numerically and experimentally measured magnetic field for the square structure. One can see the presence of pronounced fringes due to the interference of incident and reflected waves. However, as discussed in Section 2.2, when asymptotes of the dispersion contour are perpendicular to the edge of the hyperbolic metasurface, the reflected wave becomes highly decaying. As a result, the amplitude of the reflected wave is negligible in comparison to the amplitude of the incident wave. Therefore, the interference pattern is absent for the rhombic structure [see Figs. 4(j) and 4(l)]. It is crucial to clarify that because the dipole emits waves spanning a broad range of wave vectors, both numerical modeling and experiments reveal the presence of waves that are completely reflected from the boundaries of the sample oriented as a square [Figs. 3(b) and 3(f)] and waves that radiate into free space through the boundaries of the sample oriented as a rhombus [Figs. 3(c) and 3(k)].

3. DISCUSSION AND OUTLOOK

The results obtained show that hyperbolic medium with correctly modeled losses leads to the presence of the isofrequency contour branches in each quadrant of the k-space. However, as $\kappa \to 0$, precisely in those quadrants in which the branches of the dispersion curve are absent for the lossless hyperbolic media, the imaginary part of k_z is diverging (Fig. 2). Thus, the transition from lossy to lossless hyperbolic media is non-regular. Therefore, it is important to always consider hyperbolic media as lossy. It is important to stress that the normal component of the k-vector for the incident and reflected waves is no longer related to $k_z^i = -k_z^{\mathrm{ref}}$, as it is commonly considered. To be pre-

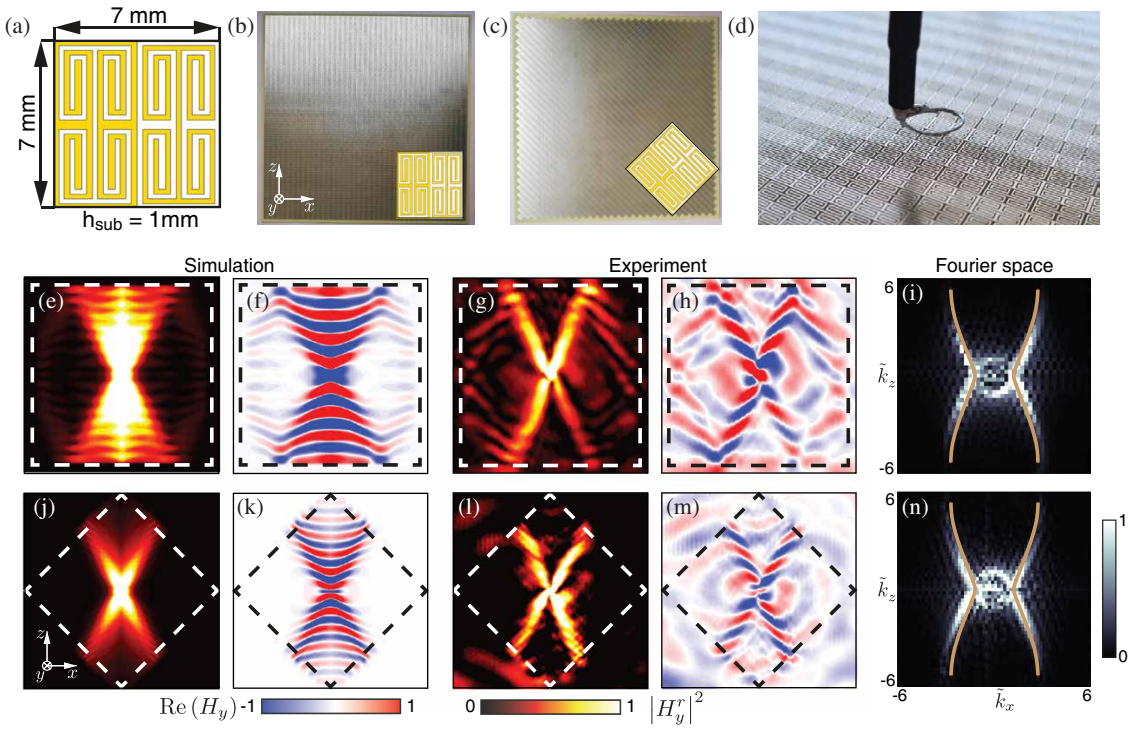

FIGURE 4. Numerical simulation and experimental results. (a) Unit cell of the metasurface. (b) Square and (c) rhombic samples, respectively. The insets show the orientation of the unit cell. (d) Photo of the excitation loop over a metasurface. Panels (e)–(i), and (j)–(n) show the magnetic field distribution obtained numerically and experimentally for the rhombic and square samples, respectively. (e), (g), (j), (l), and (f), (h), (k), (m) are the modulus and real parts of H_y, respectively. The dashed rectangles represent the edge of the sample. (i), (n) Two-dimensional Fourier transform of the experimentally measured normal component of the magnetic field for the square and rhombic samples, respectively. Brown lines correspond to the numerically calculated IFCs using the Eigenfrequency Solver of CST Microwave Studio. All experimental and simulation results are obtained for the frequency 4 GHz.

cise, for small values of κ, $k_z^{i\prime} = -k_z^{r\prime}$, but $k_z^{i\prime\prime} \sim \kappa k_x$, while $k_z^{r\prime\prime} \sim k_x/\kappa$. While the incident wave is almost non-decaying for small losses, the reflected wave decays as $e^{k_x z/\kappa}$.

Experimental results demonstrate that the wave intensity reflected from the edge of a hyperbolic metasurface is highly dependent on the edge's orientation relative to the axes of hyperbolic dispersion. When the propagation of refracted waves is prohibited, reflection becomes negligible, as evidenced by the absence of interference between the incident and reflected waves. This phenomenon can be attributed to the rapid decay of the ghost waves propagating away from the edge of a metasurface, which is induced by losses in the FR4 substrate and copper.

The theory we present and Eqs. (3)–(6) consider the hyperbolic media within effective medium approximation and accounts for loss as a small parameter. Strictly speaking, this approximation breaks down for waves whose propagation constants exceed the reciprocal lattice period of the structure. Therefore, the accurate analysis of the ghost waves requires accounting for nonlocality, i.e., the spatial dispersion. Nevertheless, as one can see from Fig. 4, the effective medium approximation demonstrates excellent agreement with experimental results. The investigation of ghost waves and their behavior beyond the effective medium approximation, considering the finite size of metamaterial unit cells and nonlocal response, remains an important and unexplored research task.

Energy band diagrams are commonly used in solid-state physics and the optics of photonic crystals to characterize the dispersion properties of these materials. In photonic crystals, photonic stop bands represent frequency intervals where the propagation of Bloch waves is forbidden. Within these intervals, the propagation constant becomes imaginary and finite, forming evanescent fields inside the crystal. In contrast, for ghost waves in hyperbolic metamaterials (HMMs), the imaginary part of the propagation constant diverges as the material losses approach zero. This distinctive behavior highlights the unique localization of ghost waves, setting them apart from conventional evanescent waves in periodic structures. While evanescent waves appear within the forbidden frequency range, ghost waves arise within specific sectors of the k-space where propagation is forbidden.

The developed equations remain valid under the substitution $\kappa \to -\kappa$, which corresponds to introducing gain into the system. This implies that ghost waves can exhibit extremely large field amplification even for small values of κ. This opens promising opportunities for applications of ghost waves for lasing and polaritonics [60]. It is important to note that our analysis focuses on a specific case of HMM, where the ordinary and extraordinary components of the permittivity tensor have equal absolute values $\varepsilon_o = \varepsilon_e = \varepsilon$. Under this condition, the asymptotes of the HMM dispersion are orthogonal [see Fig. 2(c)]. In the more general case, where the permittivity components dif-

fer, the asymptotes intersect at an angle, dividing the k-space into two pairs of unequal sectors. One pair of these sectors corresponds to regular waves, which can propagate in a lossless HMM, while the other pair corresponds to ghost waves, which arise exclusively when material losses are introduced. Moreover, when the asymptotes are not orthogonal to the HMM interface, the reflected wave consists of a combination of regular modes and highly localized ghost modes. The presence of both components makes it experimentally challenging to isolate and distinguish the contribution of ghost modes from regular reflected waves. A reasonable and yet unresolved question is how the incident energy is redistributed among the three scattering channels in the general case: (i) transmitted waves, (ii) reflected regular waves, and (iii) ghost waves.

4. CONCLUSIONS

In this work, we analyzed and resolved the paradox of the absence of reflected waves in hyperbolic metamaterials (HMMs) and metasurfaces that appeared for specific orientations of the optical axis relative to the interface of hyperbolic media. Our analysis reveals that the resolution lies in considering the *ghost waves* — highly localized modes that emerge when losses are introduced to the hyperbolic medium. The dispersion of ghost waves lies exactly in those sectors of the k-space that are forbidden from propagating in the lossless HMM. The ghost waves remain strongly localized at the interface of HMM and demonstrate a counter-intuitive localization behavior with decreasing losses. The smaller the material losses are in HMM, the larger the imaginary part of the propagation constant of the ghost waves is and, therefore, the stronger their spatial localization is near the HMM interface. Numerical simulations and experimental measurements confirmed that, in configurations where the isofrequency contour of the hyperbolic medium is perpendicular to the interface, the reflected waves manifest themselves as ghost waves, exhibiting vanishing interference with the incident waves. The identification and characterization of ghost waves are pivotal in resolving the no-reflection paradox, as they provide the missing element to fully describe wave behavior in HMMs. Beyond addressing this fundamental issue, the insights gained from this study pave the way for practical applications, such as the development of perfect absorbers, transmitters, and low-threshold lasers that leverage the unique properties of hyperbolic media. This work underscores the critical role of loss/gain-induced effects and the proper inclusion of ghost waves in advancing our understanding and utilization of hyperbolic metamaterials.

ACKNOWLEDGEMENT

The authors thank Oleg Kotov for fruitful discussions. This work was supported by the Natural Science Foundation of China (62101154).

DECLARATION

This project was carried out during a collaboration dated 2019-2021.

APPENDIX A. ANALYTICAL DERIVATIONS

A.1. Dispersion Relation for the Lossless and Lossy Hyperbolic Media

Let us consider nonmagnetic uniaxial media described by the following permittivity tensor,

$$\hat{\varepsilon} = \begin{bmatrix} \varepsilon_{xx} & 0 & \varepsilon_{xz} \\ 0 & \varepsilon_{yy} & 0 \\ \varepsilon_{zx} & 0 & \varepsilon_{zz} \end{bmatrix}.$$

The dispersion equation for electromagnetic waves in such media can be found by solving the following equation

$$\det\left[k^2\hat{\mathbb{I}} - \mathbf{k}\otimes\mathbf{k} - \hat{\varepsilon}k_0^2\right] = 0, \tag{A1}$$

where $\mathbf{k} = [k_x, k_y, k_z]^T$ is the wavevector, and k_0 is the wavenumber in the free-space. Under the assumption $k_y = 0$, Eq. (A1) factorizes and gives the dispersion of TE- and TM-polarized waves

$$\begin{aligned} &\text{TE:} \quad k_x^2 + k_z^2 - \varepsilon_{yy}k_0^2 = 0 \\ &\text{TM:} \quad \varepsilon_{xx}k_x^2 + (\varepsilon_{xz}+\varepsilon_{zx})k_xk_z + \varepsilon_{zz}k_z^2 - \eta k_0^2 = 0 \end{aligned} \tag{A2}$$

where $\eta = \mathrm{Det}\,\hat{\varepsilon}_{2\mathrm{D}}$,

$$\hat{\varepsilon}_{2\mathrm{D}} = \begin{bmatrix} \varepsilon_{xx} & \varepsilon_{xz} \\ \varepsilon_{zx} & \varepsilon_{zz} \end{bmatrix}. \tag{A3}$$

Thus, for TM-polarized wave, one can derive

$$k_{z_\pm} = -\frac{1}{2\varepsilon_{zz}}\left[\left(\varepsilon_{xz}+\varepsilon_{zx}\right)k_x \mp\sqrt{4\varepsilon_{zz}\eta k_0^2 + \left(\left(\varepsilon_{xz}+\varepsilon_{zx}\right)^2 - 4\varepsilon_{xx}\varepsilon_{zz}\right)k_x^2}\right] \tag{A4}$$

In the case of lossless hyperbolic media with permittivity tensor $\hat{\varepsilon} = \mathrm{diag}\,[\varepsilon, \varepsilon, -\varepsilon]$, $\varepsilon \in \mathbb{R}$, rotation of the material by $\pi/4$ will result in the following transformation of $\hat{\varepsilon}$

$$\hat{\varepsilon} = \hat{\mathrm{R}}\,(\pi/4)^{\mathrm{T}}\begin{bmatrix} \varepsilon & 0 & 0 \\ 0 & \varepsilon & 0 \\ 0 & 0 & -\varepsilon \end{bmatrix}\hat{\mathrm{R}}\,(\pi/4) = \begin{bmatrix} 0 & 0 & \varepsilon \\ 0 & \varepsilon & 0 \\ \varepsilon & 0 & 0 \end{bmatrix}, \tag{A5}$$

where

$$\hat{\mathrm{R}}\,(\theta) = \begin{bmatrix} \cos\theta & 0 & \sin\theta \\ 0 & 1 & 0 \\ -\sin\theta & 0 & \cos\theta \end{bmatrix}. \tag{A6}$$

Substitution of Eq. (A5) into Eq. (A4) will give the following relation between k_z and k_x components of the wavevector of the TM-polarized wave

$$k_z = -\frac{1}{2}\frac{\varepsilon}{k_x}k_0^2. \tag{A7}$$

One can see that isofrequency contours in this case are hyperbolas. However, if losses are present in the system, the relation between k_z and k_x is changed drastically. Let us introduce x arbitrary losses to the hyperbolic medium, $\pm\varepsilon \to \pm\varepsilon + i\kappa$, $\varepsilon, \kappa \in \mathbb{R}$. Then,

$$\hat{\varepsilon} = \hat{\mathrm{R}}\left(\pi/4\right)^{\mathrm{T}} \begin{bmatrix} \varepsilon + i\kappa & 0 & 0 \\ 0 & \varepsilon + i\kappa & 0 \\ 0 & 0 & -\varepsilon + i\kappa \end{bmatrix} \hat{\mathrm{R}}\left(\pi/4\right)$$

$$= \begin{bmatrix} i\kappa & 0 & \varepsilon \\ 0 & \varepsilon + i\kappa & 0 \\ \varepsilon & 0 & i\kappa, \end{bmatrix}. \tag{A8}$$

In this case the relation between k_x and k_z components is

$$k_{z_\pm} = \frac{i}{\kappa}\left[k_x\varepsilon \pm \sqrt{(k_x^2 - i\kappa k_0^2)(\kappa^2 + \varepsilon^2)}\right]. \tag{A9}$$

A.2. Refraction Coefficients for the Interface between Uniaxial and Isotropic Media

Let us consider the problem of refraction of a plane electromagnetic wave at the interface between uniaxial media with material parameters

$$\hat{\varepsilon} = \begin{bmatrix} \varepsilon_{xx} & 0 & \varepsilon_{xz} \\ 0 & \varepsilon_{yy} & 0 \\ \varepsilon_{zx} & 0 & \varepsilon_{zz} \end{bmatrix}, \tag{A10}$$

$\mu = 1$, and isotropic dielectric with material parameters ε_d, $\mu_d = 1$. We are interested in the refraction of the TM-polarized wave. The coordinate system is chosen in such a way that the electric field of the incident wave lies in the xz plane. Boundary conditions for the interface between media "1" and media "2" (if there are no surface charges and currents) are

$$\begin{aligned} E_\tau^{(1)} - E_\tau^{(2)} = 0, \quad H_\tau^{(1)} - H_\tau^{(2)} = 0, \\ D_n^{(1)} - D_n^{(2)} = 0, \quad B_n^{(1)} - B_n^{(2)} = 0, \end{aligned} \tag{A11}$$

where τ and n denote transversal and normal, with respect to the interface, and components of fields. In Cartesian coordinates, boundary conditions for the electric field will have the following look

$$E_x^i + E_x^{\mathrm{ref}} = E_x^t, \tag{A12}$$

and

$$D_z^i + D_z^{\mathrm{ref}} = D_z^t. \tag{A13}$$

Under substitution of the material equation $\mathbf{D} = \hat{\varepsilon}\mathbf{E}$, Eq. (A13) rewrites as

$$\left(\varepsilon_{zx}E_x^i + \varepsilon_{zz}E_z^i\right) + \left(\varepsilon_{zx}E_x^{\mathrm{ref}} + \varepsilon_{zz}E_z^{\mathrm{ref}}\right) = \varepsilon_d E_z^t. \tag{A14}$$

Using the Gauss law $\nabla \cdot \mathbf{D} = 0$, it is possible to show that

$$E_z = -\frac{k_x\varepsilon_{xx} + k_z\varepsilon_{zx}}{k_x\varepsilon_{xz} + k_z\varepsilon_{zz}}E_x. \tag{A15}$$

Therefore, Eq. (A14) can be simplified as follows

$$\left(\varepsilon_{zx} - \varepsilon_{zz}\frac{k_x\varepsilon_{xx} + k_z^i\varepsilon_{zx}}{k_x\varepsilon_{xz} + k_z^i\varepsilon_{zz}}\right)E_x^i + \left(\varepsilon_{zx} - \varepsilon_{zz}\frac{k_x\varepsilon_{xx} + k_z^{\mathrm{ref}}\varepsilon_{zx}}{k_x\varepsilon_{xz} + k_z^{\mathrm{ref}}\varepsilon_{zz}}\right)E_x^{\mathrm{ref}} = -\varepsilon_d\frac{k_x}{k_z^t}E_x^t, \tag{A16}$$

where we used the fact that isotropy of space in x direction implies that momentum in that direction is conserved, i.e.,

$$k_x^i = k_x^{\mathrm{ref}} = k_x^t = k_x. \tag{A17}$$

Substitution of E_x^t from Eq. (A12) into Eq. (A16) gives following equation

$$\left(\varepsilon_{zx} + \varepsilon_d\frac{k_x}{k_z^t} - \varepsilon_{zz}\frac{k_x\varepsilon_{xx} + k_z^i\varepsilon_{zx}}{k_x\varepsilon_{xz} + k_z^i\varepsilon_{zz}}\right)E_x^i = \left(\varepsilon_{zz}\frac{k_x\varepsilon_{xx} + k_z^{\mathrm{ref}}\varepsilon_{zx}}{k_x\varepsilon_{xz} + k_z^{\mathrm{ref}}\varepsilon_{zz}} - \varepsilon_{zx} - \varepsilon_d\frac{k_x}{k_z^t}\right)E_x^{\mathrm{ref}}. \tag{A18}$$

Thus, the reflection coefficient for the tangential component of the electric field of the TM-polarized wave, after simplification, is

$$r_x \equiv \frac{E_x^{\mathrm{ref}}}{E_x^i} = \frac{\left(\varepsilon_{xz}k_x + \varepsilon_{zz}k_z^{\mathrm{ref}}\right)\left(\eta k_z^t - \varepsilon_d\left(\varepsilon_{xz}k_x + \varepsilon_{zz}k_z^i\right)\right)}{\left(\varepsilon_{xz}k_x + \varepsilon_{zz}k_z^i\right)\left(\varepsilon_d\left(\varepsilon_{xz}k_x + \varepsilon_{zz}k_z^{\mathrm{ref}}\right) - \eta k_z^t\right)}. \tag{A19}$$

From boundary conditions, it is clear that the transmission coefficient is connected with the reflection coefficient as

$$t_x = r_x + 1. \tag{A20}$$

It can be more convenient to solve the refraction problem via the only component of the magnetic field, thus we also derive the expression for reflection and transmission coefficients for the magnetic field. From Maxwell's equations, one can obtain

$$\frac{k_z}{k_0}H_y = \varepsilon_{xx}E_x + \varepsilon_{xz}E_z, \quad -\frac{k_x}{k_0}H_y = \varepsilon_{zx}E_x + \varepsilon_{zz}E_z. \tag{A21}$$

from which it is possible to show that

$$E_x = \frac{\varepsilon_{xz}k_x + \varepsilon_{zz}k_z}{\eta}H_y, \quad E_z = -\frac{\varepsilon_{xx}k_x + \varepsilon_{zx}k_z}{\eta}H_y. \tag{A22}$$

Thus,

$$r_h \equiv \frac{H_y^{\mathrm{ref}}}{H_y^i} = \frac{\varepsilon_{zz}k_z^i + \varepsilon_{xz}k_x}{\varepsilon_{zz}k_z^{\mathrm{ref}} + \varepsilon_{xz}k_x}\frac{E_x^{\mathrm{ref}}}{E_x^i} = \frac{\varepsilon_{zz}k_z^i + \varepsilon_{xz}k_x}{\varepsilon_{zz}k_z^{\mathrm{ref}} + \varepsilon_{xz}k_x}r_x. \tag{A23}$$

The relation between the transmission and the reflection coefficient for the magnetic field is the same as for the tangential component of the electric field,

$$t_h = r_h + 1. \tag{A24}$$

APPENDIX B. NUMERICAL SIMULATIONS AND MEASUREMENTS

B.1. Numerical Simulations

For the numerical simulations, we used CST Microwave Studio 2019 software. Full-scale numerical models of both metasurface samples were built. Isofrequency curves and H-field maps for both samples were calculated using the eigenmode and transient solvers, respectively.

B.2. Experiment

In the experiment, the excitation loop was placed at the center of the metasurface sample and connected to the first port of a two-port vector network analyzer (VNA) Anritsu model MS2036C. Simultaneously, a probe loop with the same diameter as the excitation loop was connected to the second port of the VNA. The fabricated sample was mounted on a foam substrate and positioned between the excitation loop and the probe for near-field measurements. The probe loop was attached to a 3D near-field scanner, oriented parallel to the metasurface on the opposite side of the structure, with a gap of 7 mm between the probe and the sample. The measured H-field maps were then converted into isofrequency contours using a spatial Fourier transform. The discrepancy between the numerical simulations and experimental results can be attributed to the asymmetry of the excitation and probe loops, which causes asymmetry in the field profiles and imperfections in the sample.

REFERENCES

[1] Bloembergen, N. and P. S. Pershan, "Light waves at the boundary of nonlinear media," *Physical Review*, Vol. 128, No. 2, 606–622, Oct. 1962.

[2] Lekner, J., "Reflection and refraction by uniaxial crystals," *Journal of Physics: Condensed Matter*, Vol. 3, No. 32, 6121, Aug. 1991.

[3] Lekner, J., "Optical properties of isotropic chiral media," *Pure and Applied Optics: Journal of the European Optical Society Part A*, Vol. 5, No. 4, 417, 1996.

[4] Luukkonen, O., M. G. Silveirinha, A. B. Yakovlev, C. R. Simovski, I. S. Nefedov, and S. A. Tretyakov, "Effects of spatial dispersion on reflection from mushroom-type artificial impedance surfaces," *IEEE Transactions on Microwave Theory and Techniques*, Vol. 57, No. 11, 2692–2699, Nov. 2009.

[5] Yu, N., P. Genevet, M. A. Kats, F. Aieta, J.-P. Tetienne, F. Capasso, and Z. Gaburro, "Light propagation with phase discontinuities: Generalized laws of reflection and refraction," *Science*, Vol. 334, No. 6054, 333–337, Sep. 2011.

[6] Paniagua-Domínguez, R., Y. F. Yu, A. E. Miroshnichenko, L. A. Krivitsky, Y. H. Fu, V. Valuckas, L. Gonzaga, Y. T. Toh, A. Y. S. Kay, B. Luk'yanchuk, and A. I. Kuznetsov, "Generalized brewster effect in dielectric metasurfaces," *Nature Communications*, Vol. 7, No. 1, 10362, Jan. 2016.

[7] Yermakov, O., "Shift of Brewster's angle with two-dimensional materials and structures," *Physical Review A*, Vol. 109, No. 3, L031502, Mar. 2024.

[8] Liang, Y., K. Koshelev, F. Zhang, H. Lin, S. Lin, J. Wu, B. Jia, and Y. Kivshar, "Bound states in the continuum in anisotropic plasmonic metasurfaces," *Nano Letters*, Vol. 20, No. 9, 6351–6356, Jun. 2020.

[9] Jackson, J. D., *Classical Electrodynamics*, Wiley, Aug. 1998.

[10] Zengerle, R., "Light propagation in singly and doubly periodic planar waveguides," *Journal of Modern Optics*, Vol. 34, No. 12, 1589–1617, 1987.

[11] Gralak, B., S. Enoch, and G. Tayeb, "Anomalous refractive properties of photonic crystals," *Journal of the Optical Society of America A*, Vol. 17, No. 6, 1012–1020, Jun. 2000.

[12] Krishnamoorthy, H. N. S., Z. Jacob, E. Narimanov, I. Kretzschmar, and V. M. Menon, "Topological transitions in metamaterials," *Science*, Vol. 336, No. 6078, 205–209, Apr. 2012.

[13] Orlov, A. A., S. V. Zhukovsky, I. V. Iorsh, and P. A. Belov, "Controlling light with plasmonic multilayers," *Photonics and Nanostructures — Fundamentals and Applications*, Vol. 12, No. 3, 213–230, Jun. 2014.

[14] Belov, P. A., C. R. Simovski, and P. Ikonen, "Canalization of subwavelength images by electromagnetic crystals," *Physical Review B*, Vol. 71, No. 19, 193105, May 2005.

[15] Orlov, A. A., P. M. Voroshilov, P. A. Belov, and Y. S. Kivshar, "Engineered optical nonlocality in nanostructured metamaterials," *Physical Review B*, Vol. 84, No. 4, 045424, Jul. 2011.

[16] He, M., T. G. Folland, J. Duan, P. Alonso-González, S. D. Liberato, A. Paarmann, and J. D. Caldwell, "Anisotropy and modal hybridization in infrared nanophotonics using low-symmetry materials," *ACS Photonics*, Vol. 9, No. 4, 1078–1095, Mar. 2022.

[17] Poddubny, A., I. Iorsh, P. Belov, and Y. Kivshar, "Hyperbolic metamaterials," *Nature Photonics*, Vol. 7, No. 12, 948–957, Nov. 2013.

[18] Ferrari, L., C. Wu, D. Lepage, X. Zhang, and Z. Liu, "Hyperbolic metamaterials and their applications," *Progress in Quantum Electronics*, Vol. 40, 1–40, Mar. 2015.

[19] Shekhar, P., J. Atkinson, and Z. Jacob, "Hyperbolic metamaterials: Fundamentals and applications," *Nano Convergence*, Vol. 1, 1–17, Jun. 2014.

[20] Jacob, Z., J.-Y. Kim, G. V. Naik, A. Boltasseva, E. E. Narimanov, and V. M. Shalaev, "Engineering photonic density of states using metamaterials," *Applied Physics B*, Vol. 100, 215–218, Jun. 2010.

[21] Poddubny, A. N., P. A. Belov, and Y. S. Kivshar, "Spontaneous radiation of a finite-size dipole emitter in hyperbolic media," *Physical Review A*, Vol. 84, No. 2, 023807, Aug. 2011.

[22] Argyropoulos, C., N. M. Estakhri, F. Monticone, and A. Alù, "Negative refraction, gain and nonlinear effects in hyperbolic metamaterials," *Optics Express*, Vol. 21, No. 12, 15 037–15 047, Jun. 2013.

[23] Liu, Y. and X. Zhang, "Metasurfaces for manipulating surface plasmons," *Applied Physics Letters*, Vol. 103, No. 14, 141101, Sep. 2013.

[24] High, A. A., R. C. Devlin, A. Dibos, M. Polking, D. S. Wild, J. Perczel, N. P. D. Leon, M. D. Lukin, and H. Park, "Visible-frequency hyperbolic metasurface," *Nature*, Vol. 522, No. 7555, 192–196, Jun. 2015.

[25] Gomez-Diaz, J. S., M. Tymchenko, and A. Alù, "Hyperbolic plasmons and topological transitions over uniaxial metasurfaces," *Physical Review Letters*, Vol. 114, No. 23, 233901, Jun. 2015.

[26] Correas-Serrano, D., A. Alù, and J. S. Gomez-Diaz, "Plasmon canalization and tunneling over anisotropic metasurfaces," *Physical Review B*, Vol. 96, No. 7, 075436, Aug. 2017.

[27] Yermakov, O., V. Lenets, A. Sayanskiy, J. Baena, E. Martini, S. Glybovski, and S. Maci, "Surface waves on self-complementary metasurfaces: All-frequency hyperbolicity, extreme canalization, and TE-TM polarization degeneracy," *Physical Review X*, Vol. 11, No. 3, 031038, Aug. 2021.

[28] Takayama, O., E. Shkondin, A. Bodganov, M. E. A. Panah, K. Golenitskii, P. Dmitriev, T. Repän, R. Malureanu, P. Belov, F. Jensen, and A. V. Lavrinenko, "Midinfrared surface waves on a high aspect ratio nanotrench platform," *ACS Photonics*, Vol. 4, No. 11, 2899–2907, Oct. 2017.

[29] Hassani Gangaraj, S. A., G. W. Hanson, M. G. Silveirinha, K. Shastri, M. Antezza, and F. Monticone, "Unidirectional and diffractionless surface plasmon polaritons on three-dimensional nonreciprocal plasmonic platforms," *Physical Review B*, Vol. 99, No. 24, 245414, Jun. 2019.

[30] Nemilentsau, A., T. Stauber, G. Gómez-Santos, M. Luskin, and T. Low, "Switchable and unidirectional plasmonic beacons in hyperbolic two-dimensional materials," *Physical Review B*, Vol. 99, No. 20, 201405, May 2019.

[31] Yermakov, O. Y., A. I. Ovcharenko, M. Song, A. A. Bogdanov, I. V. Iorsh, and Y. S. Kivshar, "Hybrid waves localized at hyperbolic metasurfaces," *Physical Review B*, Vol. 91, No. 23, 235423, Jun. 2015.

[32] Yermakov, O. Y., A. A. Hurshkainen, D. A. Dobrykh, P. V. Kapitanova, I. V. Iorsh, S. B. Glybovski, and A. A. Bogdanov, "Experimental observation of hybrid TE-TM polarized surface waves supported by a hyperbolic metasurface," *Physical Review B*, Vol. 98, No. 19, 195404, Nov. 2018.

[33] Li, M., G. Hu, X. Chen, C.-W. Qiu, H. Chen, and Z. Wang, "Topologically reconfigurable magnetic polaritons," *Science Advances*, Vol. 8, No. 50, eadd6660, Dec. 2022.

[34] Fang, N., H. Lee, C. Sun, and X. Zhang, "Sub-diffraction-limited optical imaging with a silver superlens," *Science*, Vol. 308, No. 5721, 534–537, Apr. 2005.

[35] Jacob, Z., L. V. Alekseyev, and E. Narimanov, "Optical hyperlens: Far-field imaging beyond the diffraction limit," *Optics Express*, Vol. 14, No. 18, 8247–8256, Sep. 2006.

[36] Gomez-Diaz, J. S. and A. Alù, "Flatland optics with hyperbolic metasurfaces," *ACS Photonics*, Vol. 3, No. 12, 2211–2224, Nov. 2016.

[37] Sreekanth, K. V., T. Biaglow, and G. Strangi, "Directional spontaneous emission enhancement in hyperbolic metamaterials," *Journal of Applied Physics*, Vol. 114, No. 13, 134306, Oct. 2013.

[38] Lu, D., J. J. Kan, E. E. Fullerton, and Z. Liu, "Enhancing spontaneous emission rates of molecules using nanopatterned multilayer hyperbolic metamaterials," *Nature Nanotechnology*, Vol. 9, No. 1, 48–53, Jan. 2014.

[39] Sreekanth, K. V., Y. Alapan, M. ElKabbash, E. Ilker, M. Hinczewski, U. A. Gurkan, A. D. Luca, and G. Strangi, "Extreme sensitivity biosensing platform based on hyperbolic metamaterials," *Nature Materials*, Vol. 15, No. 6, 621–627, Mar. 2016.

[40] Sreekanth, K. V., Y. Alapan, M. ElKabbash, A. M. Wen, E. Ilker, M. Hinczewski, U. A. Gurkan, N. F. Steinmetz, and G. Strangi, "Enhancing the angular sensitivity of plasmonic sensors using hyperbolic metamaterials," *Advanced Optical Materials*, Vol. 4, No. 11, 1767–1772, Nov. 2016.

[41] Shkondin, E., T. Repän, M. E. A. Panah, A. V. Lavrinenko, and O. Takayama, "High aspect ratio plasmonic nanotrench structures with large active surface area for label-free mid-infrared molecular absorption sensing," *ACS Applied Nano Materials*, Vol. 1, No. 3, 1212–1218, Feb. 2018.

[42] Yermakov, O. Y., A. I. Ovcharenko, A. A. Bogdanov, I. V. Iorsh, K. Y. Bliokh, and Y. S. Kivshar, "Spin control of light with hyperbolic metasurfaces," *Physical Review B*, Vol. 94, No. 7, 075446, Aug. 2016.

[43] Mazor, Y. and A. Alù, "Routing optical spin and pseudospin with metasurfaces," *Physical Review Applied*, Vol. 14, No. 1, 014029, Jul. 2020.

[44] Kapitanova, P. V., P. Ginzburg, F. J. Rodríguez-Fortuño, D. S. Filonov, P. M. Voroshilov, P. A. Belov, A. N. Poddubny, Y. S. Kivshar, G. A. Wurtz, and A. V. Zayats, "Photonic spin hall effect in hyperbolic metamaterials for polarization-controlled routing of subwavelength modes," *Nature Communications*, Vol. 5, No. 1, 3226, Feb. 2014.

[45] Takayama, O., J. Sukham, R. Malureanu, A. V. Lavrinenko, and G. Puentes, "Photonic spin Hall effect in hyperbolic metamaterials at visible wavelengths," *Optics Letters*, Vol. 43, No. 19, 4602–4605, Oct. 2018.

[46] Kim, M., D. Lee, T. H. Kim, Y. Yang, H. J. Park, and J. Rho, "Observation of enhanced optical spin hall effect in a vertical hyperbolic metamaterial," *ACS Photonics*, Vol. 6, No. 10, 2530–2536, Sep. 2019.

[47] Hu, G., A. Krasnok, Y. Mazor, C.-W. Qiu, and A. Alù, "Moiré hyperbolic metasurfaces," *Nano Letters*, Vol. 20, No. 5, 3217–3224, 2020.

[48] Hu, G., Q. Ou, G. Si, Y. Wu, J. Wu, Z. Dai, A. Krasnok, Y. Mazor, Q. Zhang, Q. Bao, C.-W. Qiu, and A. Alù, "Topological polaritons and photonic magic angles in twisted α-MoO_3 bilayers," *Nature*, Vol. 582, No. 7811, 209–213, 2020.

[49] Zhang, X., C. Bian, Z. Gong, R. Chen, T. Low, H. Chen, and X. Lin, "Hybrid surface waves in twisted anisotropic heterometasurfaces," *Physical Review Applied*, Vol. 21, No. 6, 064034, 2024.

[50] Rustomji, K., R. Abdeddaim, J. Achard, M. Chmiaa, E. Georget, M. Goniche, W. Helou, J. Hillairet, S. Enoch, and G. Tayeb, "Mimicking electromagnetic wave coupling in tokamak plasma with fishnet metamaterials," *Scientific Reports*, Vol. 8, No. 1, 5841, Apr. 2018.

[51] Takayama, O. and A. V. Lavrinenko, "Optics with hyperbolic materials," *Journal of the Optical Society of America B*, Vol. 36, No. 8, F38–F48, Aug. 2019.

[52] Guo, Z., H. Jiang, and H. Chen, "Hyperbolic metamaterials: From dispersion manipulation to applications," *Journal of Applied Physics*, Vol. 127, No. 7, 071101, Feb. 2020.

[53] Caldwell, J. D., A. V. Kretinin, Y. Chen, V. Giannini, M. M. Fogler, Y. Francescato, C. T. Ellis, J. G. Tischler, C. R. Woods, A. J. Giles, M. Hong, K. Watanabe, T. Taniguchi, S. A. Maier, and K. S. Novoselov, "Sub-diffractional volume-confined polaritons in the natural hyperbolic material hexagonal boron nitride," *Nature Communications*, Vol. 5, No. 1, 5221, Oct. 2014.

[54] Nemilentsau, A., T. Low, and G. Hanson, "Anisotropic 2D materials for tunable hyperbolic plasmonics," *Physical Review Letters*, Vol. 116, No. 6, 066804, Feb. 2016.

[55] Dai, S., M. Tymchenko, Y. Yang, Q. Ma, M. Pita-Vidal, K. Watanabe, T. Taniguchi, P. Jarillo-Herrero, M. M. Fogler, A. Alù, and D. N. Basov, "Manipulation and steering of hyperbolic surface polaritons in hexagonal boron nitride," *Advanced Materials*, Vol. 30, No. 16, 1706358, Apr. 2018.

[56] Li, P., I. Dolado, F. J. Alfaro-Mozaz, F. Casanova, L. E. Hueso, S. Liu, J. H. Edgar, A. Y. Nikitin, S. Vélez, and R. Hillenbrand, "Infrared hyperbolic metasurface based on nanostructured van der Waals materials," *Science*, Vol. 359, No. 6378, 892–896, Feb. 2018.

[57] Wang, H., Y. Zhong, W. Jiang, S. Latini, S. Xia, T. Cui, Z. Li, T. Low, and F. Liu, "Strain-tunable hyperbolic exciton polaritons in monolayer black arsenic with two exciton resonances," *Nano Letters*, Vol. 24, No. 6, 2057–2062, 2024.

[58] Yermakov, O. Y., D. V. Permyakov, F. V. Porubaev, P. A. Dmitriev, A. K. Samusev, I. V. Iorsh, R. Malureanu, A. V. Lavrinenko, and A. A. Bogdanov, "Effective surface conductivity

of optical hyperbolic metasurfaces: From far-field characterization to surface wave analysis," *Scientific Reports*, Vol. 8, No. 1, 14135, Sep. 2018.

[59] Guo, Z., H. Jiang, and H. Chen, "Abnormal wave propagation in tilted linear-crossing metamaterials," *Advanced Photonics Research*, Vol. 2, No. 1, 2000071, Jan. 2021.

[60] He, Z., H. Wang, Z. Cui, S. Xia, X. Tang, B. Zheng, X. Lin, L. Shen, H. Chen, and Y. Wu, "Reflectionless refraction via one-dimensional ghost polaritons in planar junctions of hyperbolic metasurfaces," *Progress In Electromagnetics Research*, Vol. 181, 1–8, 2024.

[61] Dai, Z., G. Hu, G. Si, Q. Ou, Q. Zhang, S. Balendhran, F. Rahman, B. Y. Zhang, J. Z. Ou, G. Li, A. Alù, C.-W. Qiu, and Q. Bao, "Edge-oriented and steerable hyperbolic polaritons in anisotropic van der Waals nanocavities," *Nature Communications*, Vol. 11, No. 1, 6086, Nov. 2020.